

Limits on WIMP dark matter using scintillating CaWO₄ cryogenic detectors with active background suppression

G. Angloher ^a, C. Bucci ^d, P. Christ ^a, C. Cozzini ^b, F. von Feilitzsch ^c,
 D. Hauff ^a, S. Henry ^b, Th. Jagemann ^c, J. Jochum ^e, H. Kraus ^b,
 B. Majorovits ^b, J. Ninkovic ^a, F. Petricca ^a, W. Potzel ^c, F. Pröbst ^{a, +},
 Y. Ramachers ^{b, *}, M. Razeti ^c, W. Rau ^c, W. Seidel ^a, M. Stark ^c,
 L. Stodolsky ^a, A. J. B. Tolhurst ^b, W. Westphal ^c, H. Wulandari ^c

^a *MPI für Physik, Föhringer Ring 6, 80805 Munich, Germany*

^b *University of Oxford, Department of Physics, Oxford OX1 3RH, U.K.*

^c *Technische Universität München, Physik Department, D-85747 Garching, Germany*

^d *Laboratori Nazionali del Gran Sasso, I-67010 Assergi, Italy*

^e *Eberhard-Karls-Universität Tübingen, D-72076 Tübingen, Germany*

⁺ *corresponding author: probst@mppmu.mpg.de*

^{*} *present address: University of Warwick, Coventry CV4 7AL, U.K.*

WIMPs; dark matter; low temperature detectors; CaWO₄; background discrimination

Abstract

We present first significant limits on WIMP dark matter by the phonon-light technique, where combined phonon and light signals from a scintillating cryogenic detector are used. Data from early 2004 with two 300 g CRESST-II prototype detector modules are presented, with a net exposure of 20.5 kg days. The modules consist of a CaWO₄ scintillating “target” crystal and a smaller cryogenic light detector. The combination of phonon and light signals leads to a strong suppression of non-nuclear recoil backgrounds. Using this information to define an acceptance region for nuclear recoils we have 16 events from the two modules, corresponding to a rate for nuclear recoils between 12 and 40 keV of (0.87 ± 0.22) events/(kg day). This is compatible with the rate expected from neutron background, and most of these events lie in the region of the phonon-light plane anticipated for neutron-induced recoils. A particularly strong limit for WIMPs with coherent scattering results from selecting a region of the phonon-light plane corresponding to tungsten recoils, where the best module shows zero events.

1 Introduction

Despite persuasive indirect evidence for the existence of dark matter in the universe and in galaxies, the direct detection of dark matter remains one of the outstanding experimental challenges of present-day physics and cosmology.

A plausible candidate for the dark matter is the Weakly Interacting Massive Particle (WIMP) and it is possible that it can be detected by laboratory experiments, particularly using cryogenic methods, which are well adapted to the small energy deposit anticipated [1]. Supersymmetry provides a well motivated WIMP candidate in the form of the lightest supersymmetric particle. WIMPs [2] are expected to be gravitationally bound in a roughly isothermal halo around the visible part of our galaxy with a density of about 0.3 GeV/cm^3 at the position of the Earth [3].

Interaction with ordinary matter is expected via elastic scattering on nuclei. The elastic nuclear scattering can occur via coherent (“spin independent”) or spin-dependent interactions. For the coherent case, a factor A^2 is expected in the cross section, favoring heavy nuclei [4]. We present our WIMP limits in terms of this possibility.

In the CRESST experiment we attempt to detect the WIMP-nucleus scattering using cryogenic methods. Results from the first phase of CRESST using sapphire (Al_2O_3) detectors have been previously reported, see ref. [5]. For the second phase [6] presently in preparation, CRESST-II, we have developed cryogenic detectors based on scintillating $CaWO_4$ crystals. When supplemented with a light detector these provide very efficient discrimination of nuclear recoils from radioactive γ and β backgrounds, down to recoil energies of about 10 keV. The heaviest nucleus in our crystal is tungsten, for which the recoil energy is expected to reach up to about 40 keV, with rates below 1 event/(kg day). The mass of each crystal is about 300 g. Data were accumulated with two of these prototype detector modules during 53 days between January 31 and March 23 of 2004 at the Laboratori Nazionali del Gran Sasso (LNGS).

Passive background suppression is achieved with a low background installation and the deep underground location. The overburden of 3500 meter water equivalent at the LNGS leads to a reduction of the surface muon flux by 10^6 to about $1/(\text{m}^2 \text{ h})$, while the detectors themselves are shielded against ambient radioactivity by thicknesses of 14 cm of low background copper and 20 cm of low background lead. A neutron shield and a muon veto, to be installed for CRESST-II, were not present for the data presented here.

The setup for the prototype run reported here is the same as in CRESST-I, described in more detail in ref. [5]. A four channel SQUID system allowed the simultaneous operation of two phonon/light modules. The measurements were halted on March 23 to proceed with the upgrade, which in addition to the neutron shield and the muon veto, will involve a 66 channel SQUID readout system to enable operation of 33 detector modules [6].

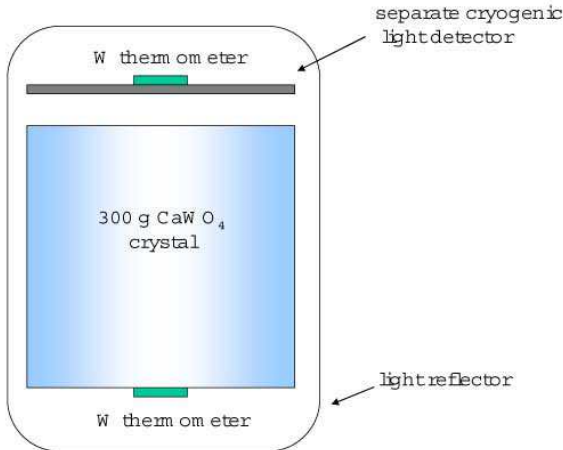


Figure 1: Schematic representation of the detector for coincident phonon and light measurement. It consists of two cryogenic detectors enclosed in a highly reflective housing, read out by tungsten superconducting phase transition thermometers.

2 Detectors

A single detector module consists of a scintillating CaWO_4 “target” crystal, operated as a cryogenic calorimeter (the “phonon channel”), and a nearby but separate cryogenic detector optimized for the detection of scintillation photons (the “light channel”). The phonon channel is designed to measure the energy transfer to a nucleus of the CaWO_4 crystal in a WIMP-nucleus elastic scattering. Since a nucleus and an electron or gamma of the same energy differ substantially in the yield of scintillation light, an effective background discrimination against gammas and electrons is obtained by a simultaneous measurement of the phonon and light signals. Among different scintillating crystals, CaWO_4 was selected because of its high light yield at low temperatures and the absence of a noticeable degradation of the light yield for events near the crystal surface [7]. Such a degradation, often found in coincident phonon-charge measurements and some scintillators, can cause difficulties as it may lead to a misidentification of electron/photon surface events as nuclear recoils. In addition, the large atomic mass ($A=183.86$) of tungsten makes CaWO_4 a very favorable target for WIMPs with coherent interactions.

The prototype detector modules used here [7, 8, 9] consist of a 300 g cylindrical CaWO_4 crystal with 40 mm diameter and height, and an associated cryogenic light detector. The light detector is mounted close to a flat surface of the CaWO_4 crystal, and both detectors are enclosed by a housing made of a highly reflective polymeric multilayer foil [10]. An important improvement of the energy resolution of the light channel was achieved by roughening the flat surface of the CaWO_4 facing the light detector to a roughness of about

$10\ \mu\text{m}$. This reduces internal total reflection and facilitates the escape of the scintillation photons to the light detector. Both detectors are read out by optimized tungsten superconducting phase transition thermometers. The arrangement is shown schematically in Fig. 1. The polymeric foil was measured to have a reflectivity of about 99 % at the wavelength of the scintillation maximum (420 nm) of CaWO_4 . In addition we have discovered that the carrier foil onto which the reflecting foil is grown is itself scintillating at low temperatures. We mounted the reflector with the carrier foil inside, facing the detectors. This is very useful in discriminating backgrounds from α decays on the crystal or reflector surfaces where the α particle goes away from the crystal and only the recoil nucleus enters the CaWO_4 crystal, with little light emission. The additional light from the α particle as it is absorbed on the facing surface of the foil allows the rejection of such events.

An early problem of no-light events induced by stress on the crystal was eliminated by replacing teflon supports with copper beryllium springs to hold the crystal. These springs were silver coated and other elements for holding the reflecting foil were made of sintered Teflon. Both materials are highly reflective in the wavelength range of interest, but do not scintillate. In future designs these elements will be coated with an organic scintillator.

The two CaWO_4 crystals used in this work were called “Julia” and “Daisy”, the associated light detectors were denoted as “BE 14” and “BE 13” respectively. The detectors are operated at a temperature of about $10\ \text{mK}$ where the tungsten thermometer is in the middle of its transition between the superconducting and the normal conducting state, so that a small temperature rise of the thermometer leads to a relatively large rise of its resistance.

The thermal response of the thermometer film can be described by a model [11] which leads to a pulse described by a rise time and two decay times. Roughly speaking, the initial high frequency phonons created by a particle or photon interaction are reflected many times at the free crystal surface to form a “hot” (relative to the initial temperature) “gas” of phonons. These athermal phonons are readily absorbed by the electrons of the thermometer. However, after thermalization of their energy in the metal the resulting thermal phonons are very weakly coupled back to the crystal. This is a kind of “greenhouse effect” due to the strongly decreasing thermal electron-phonon coupling at low temperature, $g_{e-p} \propto T^5$. This effective thermal decoupling of the crystal is important for the “thermal tuning” of the detectors in that it permits the relaxation time of the thermometer to be determined essentially by the heat capacity of the thermometer and the thermal conductance to the heat bath. The thermal time constant of the thermometer is thus adjusted via a normal conducting metallic link to the copper crystal holder, which plays the role of the “heat bath”.

The resistance of the tungsten thermometer ($\sim 0.3\ \Omega$) is measured by means of a two-armed parallel circuit carrying a total constant current of a few μA . One arm of the circuit is given by the superconducting film and the other consists of the input coil of the SQUID in series with a reference resistor ($0.05\ \Omega$), which provides a sensitive measurement of current changes. A rise in the thermometer resistance and so an increase in current through the SQUID coil is then observed as a rise in SQUID output voltage.

For the data acquisition system the output voltage of the SQUID electronics is split into two branches. In one branch the pulse is shaped and AC-coupled to a trigger unit, while in the other the signal is passed through an anti-aliasing filter and DC-coupled to a 16-bit transient digitizer. The time base of the transient digitizer was chosen to be $40\ \mu\text{s}$, providing about 30 samples for the rising part of the pulse (phonon channel). The total record length of 4096 time bins includes a “pre-trigger” region of 1024 samples to record the baseline before the event, while the “post-trigger” region of 3072 samples contains the pulse itself. The phonon and light channels were read out together, whenever one or both triggered. The transient digitizer data was then written to disk for off-line analysis. After each trigger there is a dead time of $\sim 70\ \text{ms}$ to allow for the readout and the sampling of the next pre-trigger region. Pulses from another module which arrive within half of the post-trigger period are also recorded together with the time delay with respect to the first trigger. This discarding of triggers in other modules arriving after half of the post trigger period contributes a dead time of 102.4 ms per event for these other modules. The accumulated dead time is measured with separate clocks for each channel.

In addition to data pulses, the data acquisition system also records the response to periodic heater pulses which are applied to each thermometer to record and monitor the behavior of the detectors.

2.1 Phonon channel

The thermometer of the CaWO_4 crystals is a $6 \times 8\ \text{mm}^2$, 200 nm thick superconducting tungsten film evaporated on the surface. In addition there is a buffer layer of SiO_2 between the tungsten film and the CaWO_4 to prevent interdiffusion between the tungsten film and the CaWO_4 crystal. The quite low superconducting transition temperatures of 7 mK and 9 mK for the present CaWO_4 detectors were achieved using the buffer layer and a deposition temperature of $480\ ^\circ\text{C}$. For the tungsten etching, a dilute mixture of NaH_2PO_4 , NaOH , and $\text{Na}_3\text{Fe}(\text{CN})_6$ was used instead of conventional potassium based etchants to avoid radioactive contamination by ^{40}K .

The electrical and thermal connections of the thermometer are shown in Fig. 2. Thermal connection and grounding of the detector is provided by two gold bond wires of $25\ \mu\text{m}$ diameter, connecting a gold contact pad in the middle of the tungsten film with the copper detector holder. The holder in turn is thermally connected to the mixing chamber of the dilution refrigerator, which is stabilized at 6 mK. Electrical connection is made by superconducting aluminum wires. These are bonded from the aluminum pads on each end of the thermometer to electrically insulated contact pads on the copper holder. Superconducting wires connect the contact pads to the SQUID readout circuit. These connections are screwed and not soldered to avoid the radioactivity of solder joints.

A heater for controlling the temperature of the thermometer and for injecting the test pulses is provided by a $25\ \mu\text{m}$ diameter gold wire bonded to a gold pad in the center of the thermometer and to small aluminum pads on either side of the thermometer (Fig. 2). Superconducting aluminum bond wires, with negligible thermal conductance at the low

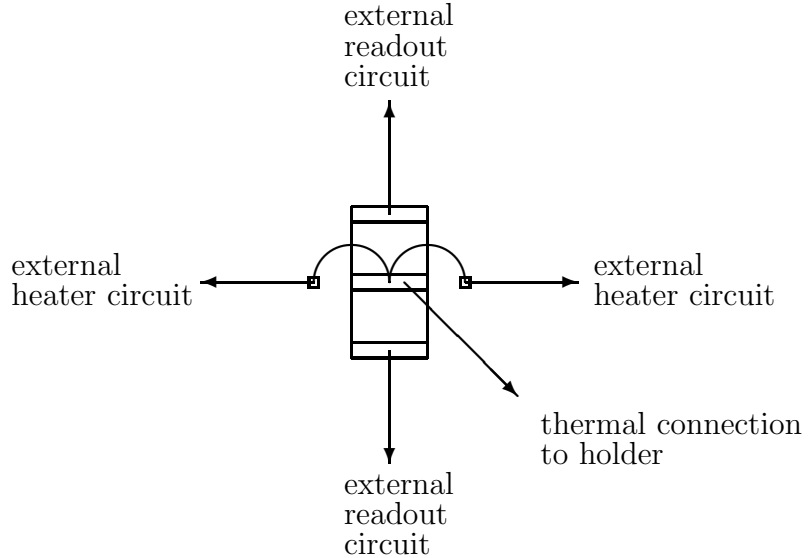


Figure 2: Schematic thermal and electrical connections to the thermometer in the phonon channel.

operating temperature, link these aluminum pads to insulated pads on the copper holder for electrical connection to the heater circuit.

2.2 Light channel

At the operating temperature, 1 % or less of the energy deposited in the CaWO_4 is detected as scintillation light. The cryogenic light detector used to detect these scintillation photons consists of a silicon wafer ($30 \times 30 \times 0.4 \text{ mm}^3$) with a tungsten thermometer. To improve the efficiency for collecting the energy of the few photons, the thermometer is supplemented by aluminum phonon collectors. This sensor, consisting of the thermometer and phonon collectors, is shown in Fig. 3. In making these sensors, an original tungsten film is covered by a superconducting $1 \mu\text{m}$ thick aluminum layer on two sides (0.5 mm^2 each), leaving a small uncovered tungsten film in the middle. This small uncovered region serves as the thermometer. The remaining aluminum/tungsten bilayer is superconducting with a transition temperature close to that of pure aluminum (1.2 K) and so has a negligible heat capacity at the operating temperature. These phonon collectors absorb high frequency athermal phonons with an efficiency similar to that of the tungsten thermometer, leading to the creation of long lived quasiparticles, which in turn efficiently deliver their energy to the tungsten thermometer [12]. In this way we obtain a large collecting area while maintaining a thermometer of small heat capacity C .

In CaWO_4 the time constant for the emission of the scintillation photons is on the order of milliseconds at mK temperatures [8]. Thus to integrate the energy of the scintillation photons a long thermal relaxation time $\tau = C/G$ is required for the light detector. A sufficiently small thermal coupling G of the thermometer to the heat bath is obtained by a 50 nm thick, $1.5 \times 0.1 \text{ mm}^2$ gold film overlapping the tungsten film at one end (lower end

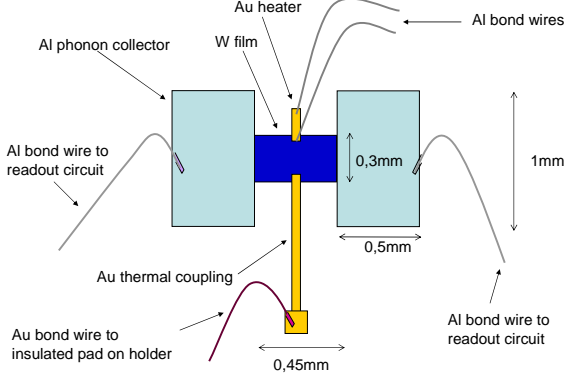


Figure 3: Thermal and electrical connections to the sensor on the light detector. Aluminum/tungsten phonon collectors surround the tungsten thermometer. Connections shown are the aluminum bond wires for electrical connection to the SQUID and heater circuits and the gold bond wire for thermal contact to the heat bath (copper holder).

in the figure 3), which is connected to the heat bath via a $25 \mu m$ gold wire bonded to an electrically insulated pad on the detector holder. The electrical insulation of this pad aids in the immunity of the detector against electronic interference. This thermal coupling scheme gives a thermal relaxation time on the order of several milliseconds. For the temperature regulation and heating test pulses, a second small gold film partially overlaps the tungsten thermometer on the other end (upper end in figure 3). It is connected via aluminum bond wires to two contact pads on the detector holder.

2.3 Temperature stability and energy calibration

Although the width of the transition from superconducting to normal resistance for a detector film is on the order of a mK, for highly stable detector response the operating point on the transition curve and so the temperature must be constant to within a few μK . Short term temperature control was maintained by using the baseline of the SQUID output voltage between pulses as the temperature indicator and then regulating the current to the heater on the thermometer. The baseline sampling rate was 10 Hz, and during a pulse the sampling was interrupted and the heater current kept constant. These processes were run under computer control with a PI-algorithm capable of recognizing pulses. This system deals with flux quantum losses in the SQUID by not responding to large ($> \phi_0/2$) jumps in SQUID baseline if they occur very quickly, namely in one sampling period.

To take care of the very rare instances when a true temperature jump has taken place in a short time, a second independent control loop provides for long term stability by checking for deviations from the desired operating point, as follows. Every two seconds, large heater pulses (~ 1.5 MeV equivalent in phonon channels), which partially saturate the detectors are injected. The energy of these pulses is large enough to drive the superconducting film

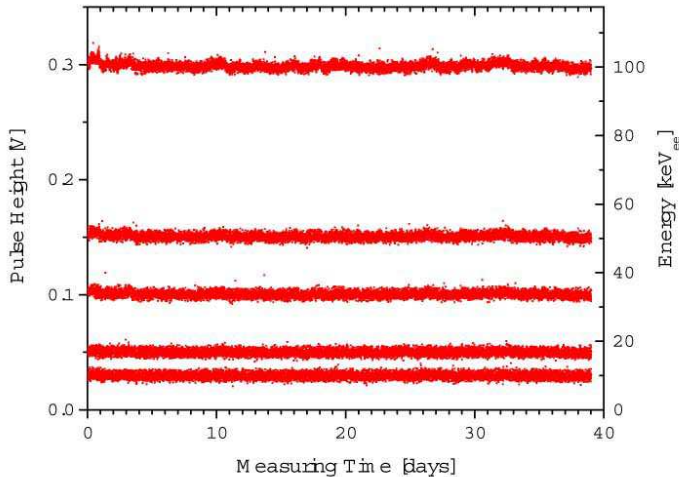


Figure 4: The measured pulse height for heater pulses on light detector BE13 as a function of time during the entire dark matter run. The energy scale on the right side refers to effective electron energy in the CaWO_4 crystal (see text). The actual energy seen by the light detector is about a factor of 100 smaller. The detector is seen to be stable within resolution.

near to the top of the transition, where it is almost normal-conducting. The resulting SQUID output voltage will thus depend on how far the operating point was from the top of the transition and a possible shift of the operating point can be recognized and corrected. Hence for each thermometer there is effectively a temperature standard given by the response of the film to a large heater pulse. The few short periods with noticeable deviations from the operating point are cut from the data. In Table 2 this is called the “stability cut”.

The same heater as used for the temperature regulation is also used to inject the periodic heater pulses which monitor the long term stability of the energy calibration and measure the trigger efficiency close to threshold. These heater pulses are produced by exponential voltage pulses from a pulser module, with the decay time adjusted to create detector pulses resembling particle pulses. The voltage for regulating the temperature and the heater pulses are added and passed through an analog square-root circuit to obtain a linear dependence of the injected heater energy vs. the amplitude of the pulser voltage. Test pulses with a number of discrete energies spanning the energy range of interest were sent every 30 s throughout both dark matter and calibration runs. Fig. 4 shows the stability of the light detector BE 13 during the entire dark matter run.

The energy corresponding to a pulse is determined by the pulse height. This in turn is found by a template fit procedure. For each detector a template is made by averaging many measured pulses of a given type, i.e. test pulses or pulses from 122 keV γ 's from the calibration source in the case of the CaWO_4 phonon detector. The pulse height of a given signal is then found by fitting the template with an amplitude scale factor, base line

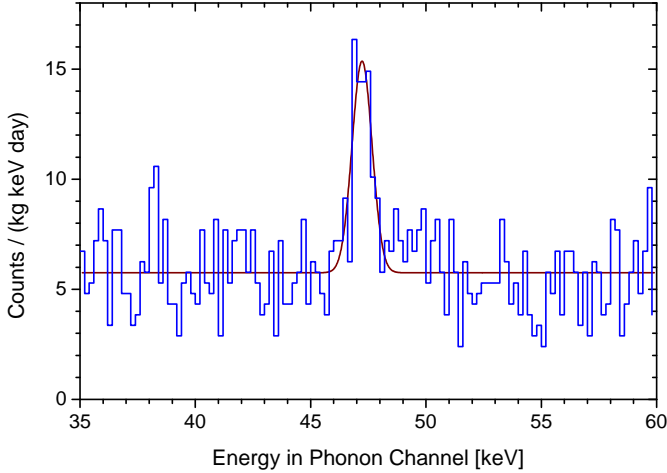


Figure 5: Peak with (3.2 ± 0.5) counts/day, of width 1.0 keV (FWHM) appearing in the phonon channel (Daisy) during the 53 day dark matter run. We attribute this peak to an ^{210}Pb contamination in the vicinity of the detectors.

and onset time as free fit parameters. The amplitude scale factor then yields the pulse height. Finally, a calibration translates the pulse height into an energy.

The CaWO₄ phonon detector, which provides the energy of an event, is calibrated with an external source to give an absolute energy determination. A ^{57}Co source (122 keV and 136 keV γ lines) is inserted into the shielding via a removable plug, illuminating the detector modules from below. Comparison of the pulse heights of the 122 keV photons with heater pulses of similar energy provides an absolute calibration for the voltage of the heater pulses in terms of an equivalent γ energy. The calibration is transferred to the lower energies needed for the WIMP analysis by means of the heater test pulses.

The accuracy of the energy calibration from 10 to 40 keV, as relevant for the WIMP search, is in the range of a few percent. This can be inferred from a peak at 47.1 keV shown in Fig. 5, which appeared in the energy spectrum of the phonon channel during the dark matter run with a rate of (3.2 ± 0.5) counts/day. If we associate this peak with the 46.54 keV γ 's from an external ^{210}Pb contamination, the calibration with the heater pulses puts it 1.2% too high. The observed accuracy of the calibration is consistent with the accuracy of the analog square-root circuit of about 1%, which is used to linearize the injected heater pulse energy with respect to the amplitude of the pulser voltage. This tendency to slightly overestimate the energy of the events will put our dark matter limits on the conservative side. The width of this peak is 1.0 keV (FWHM), identical with that for the heater pulses. This good resolution over 53 days again confirms the stability of the response during the dark matter run.

For small deposited energies the temperature rise is considerably smaller than the width of the film's superconducting transition and so we obtain an approximately linear relation

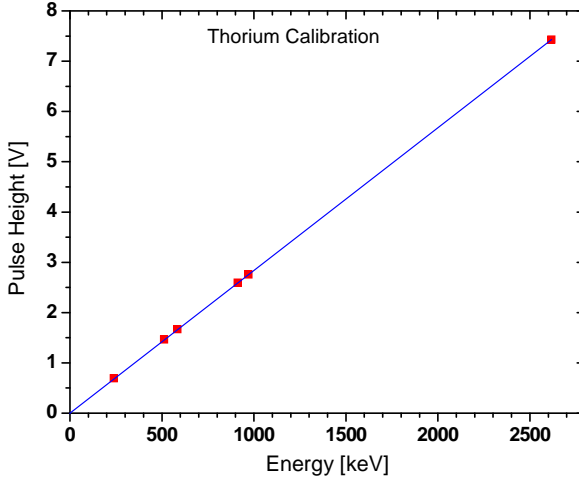


Figure 6: Measured pulse height of the phonon channel (“Daisy”) vs. energy for a set of γ peaks from a ^{232}Th source. The pulse height was determined with a truncated template fit.

between pulse amplitude and energy up to at least 170 keV in all detector channels. For larger pulses we simply exclude that part of the pulse where non-linearity sets in, and perform the fit on the thus truncated pulse. This means that large pulse heights are effectively determined by the duration of the signals. We find that the pulse heights obtained from such a truncated fit are approximately linear in energy up to several MeV.

Fig. 6 shows results obtained with a ^{232}Th calibration source. The pulse height obtained from the truncated fit procedure is plotted as a function of γ energy for a number of γ peaks of known energy. The straight line connecting the highest point with the origin serves to visualize the good linearity. A refined variant of this simple method was applied for a detailed study of the α background of the detectors. These results will be presented in a separate paper [13]. We note that the low recoil energy data used in the dark matter analysis do not involve this truncation procedure.

The hardware threshold of the detectors was set to a recoil energy of about 5 keV, and 100 % trigger efficiency was confirmed throughout the dark matter run by means of the lowest energy heater pulses, corresponding to 8.5 keV and 10 keV in the phonon channels for Julia and Daisy respectively. As mentioned, we obtain good energy resolution: $\Delta E = 1$ keV (FWHM) for 46.5 keV γ rays, $\Delta E = 1.8$ keV at 122 keV and $\Delta E = 7$ keV for 2.3 MeV α 's. Typical pulse shape parameters are $\tau_{rise} = 1.1$ ms for the rise time and $\tau_{dec} = 15$ ms for the fast decay time. At energies of a few tens of keV where the WIMP signal is expected, a background count rate of ~ 6 electron/photon events / (kg keV day), before rejection by the light signal, is obtained.

The calibration of the light detectors follows the same procedure. However, since we are not concerned with an absolute energy determination, the calibration is provided by

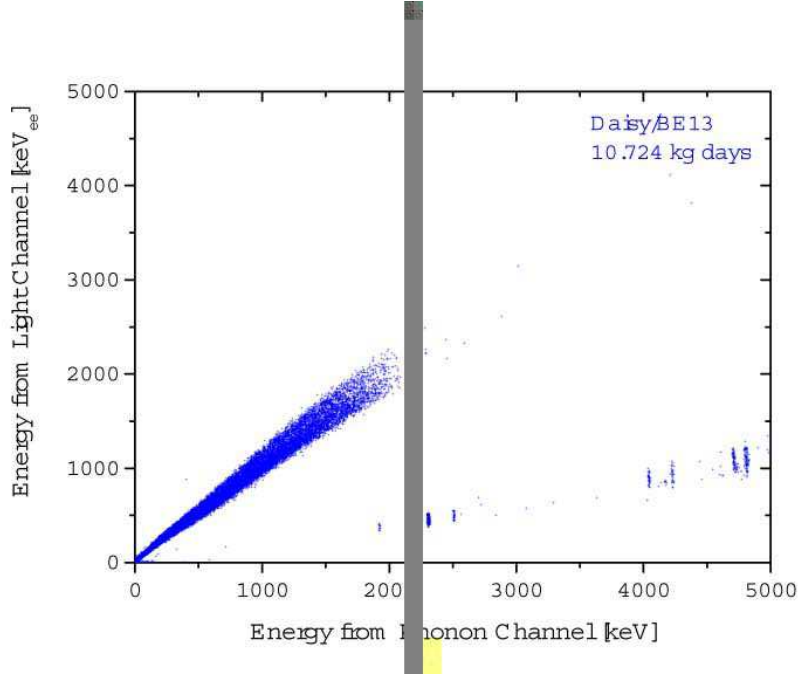


Figure 7: Energy in the light channel vs. energy in the phonon channel recorded with the module Daisy/BE13. The uniform upper band is from γ and β interactions in the CaWO₄ crystal, the lower band shows a series of discrete α peaks, mostly from the natural decay chains.

the light output of the main detector with incident 122 keV γ 's. Thus the pulse height produced in the light detector with 122 keV photons incident on the main detector is assigned the nominal value (“electron equivalents -ee”) of 122 keV.

2.4 Energy resolution of the light channel

The energy resolution of the light channel plays an important role in the analysis. It reflects not only the performance of the thermometer system but also fluctuations in light production and collection. In Fig. 7 a scatter plot of energy in the light channel vs. energy in the phonon channel over a wide energy range from Daisy/BE13 in the dark matter run is shown. Besides the continuous γ band a series of discrete α lines is visible in a band with lower light yield. These α peaks are identified and discussed in detail in [13].

Table 1: Polynomial coefficients describing the energy dependence of the energy resolution of the light channels BE13 and BE14 in the energy range from 0 to 300 keV.

Detector	A_0 [keV _{ee}]	A_1	A_2 [keV _{ee} ⁻¹]	A_3 [keV _{ee} ⁻²]
BE13	1.974	0.24347	-0.5794 10 ⁻³	0.1368 10 ⁻⁵
BE14	3.446	0.24218	-0.1617 10 ⁻³	-0.7127 10 ⁻⁷

The increasing width with energy of the γ band, as seen in Fig. 7, arises from an almost linear energy dependence of the light channel resolution. This may result from a slight dependence of the light output with respect to the position of the energy deposition within the CaWO₄ crystal. Therefore we use data from the ²³²Th calibration to extract the energy dependence of the resolution, since in these data the low energy continuum originates from Compton scattered high energy γ 's, which interact uniformly in the volume of the crystal and so are spatially distributed as expected for neutron or WIMP-induced events. The resolution in the light channel for this thorium data was modeled by a power series

$$\Delta E = \sum_{i=0}^3 A_i E^i, \quad (1)$$

for energies between zero and 300 keV, yielding the coefficients listed in Table 1. We observe that BE13 has the better resolution at low energy as indicated by the smaller value of A_0 .

The electronic noise of the better light detector and hence its energy resolution when extrapolated to zero energy, is about 2 keV (FWHM) in agreement with the energy resolution of the heater pulses. This energy resolution compares favorably with photomultipliers, which may reach about the same performance with the best scintillating crystals of NaI(Tl).

3 Results and discussion

In late 2002 and early 2003 a number of short runs were undertaken to optimize the prototype CRESST-II modules. We report here on data taken with two detector modules during the period from January 31 to March 23, 2004. Table 2 summarizes the measurement time, dead time, the time removed by the stability cut and the resulting total exposure.

Table 2: Measurement Times and Exposures

module	measuring time [days]	dead time [days]	stability cut [days]	mass [grams]	total exposure [kg days]
Julia/BE14	37.572	3.391	0.518	291.4	9.809
Daisy/BE13	39.043	3.469	0.621	306.8	10.724

Before this dark matter run the detectors were calibrated with a ⁵⁷Co source as described above and following the run the ²³²Th test reported in Fig. 6 was performed.

3.1 Nuclear recoil acceptance region

The data from the dark matter run is presented in Fig. 8. The low energy region for the two modules is shown in scatter plots where the vertical axis is the light to phonon

energy ratio, while the horizontal axis gives the phonon or total energy. The points with negative energy arise in the pulse fitting procedure when a negative amplitude results for small pulses close to the noise.

The determination of a nuclear recoil acceptance region in the phonon-light plane is based on a knowledge of the “quenching factor”, i.e. the reduction of the light output of a nuclear recoil event relative to an electron/photon event of the same energy. For this calculation we use the quenching factor $Q=7.4$, as measured with neutrons from an $^{241}\text{Am-Be}$ source [7]. A slightly higher quenching factor has been reported by another group [14], but using the smaller value of $Q=7.4$ will put our dark matter limits on the conservative side. Using this quenching factor and assuming Gaussian fluctuations parameterized with the energy resolution of the light and phonon channels, we obtain the dashed lines on the plots of Fig. 8. The upper dashed line gives the boundary below which 90 % of the nuclear recoils are expected. We also show the boundary below which 10 % of the recoils for $Q = 7.4$ are expected. This is indicated by the lower dashed lines. Since $Q = 7.4$ refers to incident neutrons, the area between the 90 % and 10 % lines will give an impression of where the neutron background is expected to lie. This 10 % line does not enter into the calculation of the WIMP limits themselves, however.

Since these calculations used the light channel resolutions from Table 1, determined with photons on the CaWO_4 detector, they also involve the assumption that the resolution of the light channel does not depend on the deposition process. We can check this assumption by comparing the light channel resolution in the two bands of Fig. 7 at the same value of the light output. If we do this at the nominal light output of 484 keV_{ee} , corresponding to the α line at 2.31 MeV, we find $64 \pm 7 \text{ keV}$ in the α band and $77 \pm 8 \text{ keV}$ in the electron/photon band; so within errors the resolutions are consistent.

Finally, an analysis threshold of 12 keV was chosen in order to stay well above the energy where electron and nuclear recoil bands intersect. The upper energy for the analysis was chosen to be 40 keV, since due to the suppression of higher energy recoils by form factor effects, more than 95 % of all WIMP induced tungsten recoils are expected below this energy for any WIMP mass. This is shown in Fig. 9. Thus our nuclear recoil acceptance region on the plots of Fig. 8 are below the upper dashed lines and from 12 to 40 keV in the phonon or total energy channel.

In this acceptance region there are a total of 7 (Daisy) and 9 (Julia) events for the two modules. Using the exposures of Table 2 and these 16 event we obtain the rate

$$R(\text{nuclear recoils}) = (0.87 \pm 0.22) / (\text{kg day}), \quad (2)$$

for $12 \text{ keV} \leq E_{\text{recoil}} \leq 40 \text{ keV}$. A 10 % acceptance correction has been applied to compensate for recoil events lost by the 90 % cut.

We note that most of these events lie between the 90 % and 10 % curves for $Q = 7.4$ and so are in the region expected for neutron-induced recoils. Furthermore, Monte Carlo simulations for our setup without neutron shielding [15] yield an estimate for the neutron background of about 0.6 events/(kg day) for $12 \text{ keV} \leq E_{\text{recoil}} \leq 40 \text{ keV}$, in reasonable agreement with Eq. 2. Both these remarks suggest the observed events are due to neutron background.

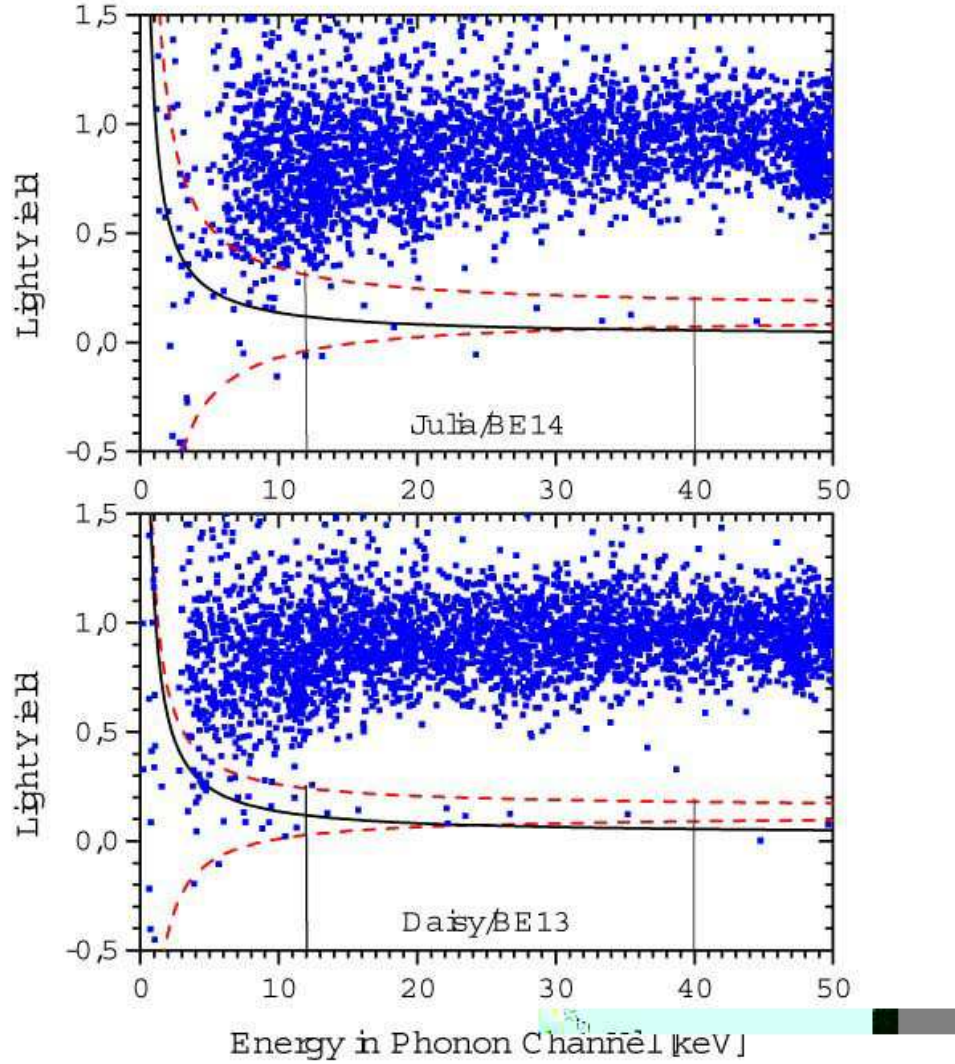


Figure 8: Low energy event distributions in the dark matter run for the two modules Julia/BE14 (top) and Daisy/BE13 (bottom). The vertical axis represents the light yield expressed as the ratio (energy in the light channel/energy in the phonon channel), and the horizontal axis the energy in the phonon channel. Taking a quenching factor of 7.4 for nuclear recoils, the region below the upper dashed curves will contain 90 % of the nuclear recoils. The lower dashed curved shows the 10 % boundary with this quenching factor. Taking a quenching factor of 40 for tungsten, the region below the solid curves will contain 90 % of tungsten recoils. The vertical lines indicate the energy range used for the WIMP analysis

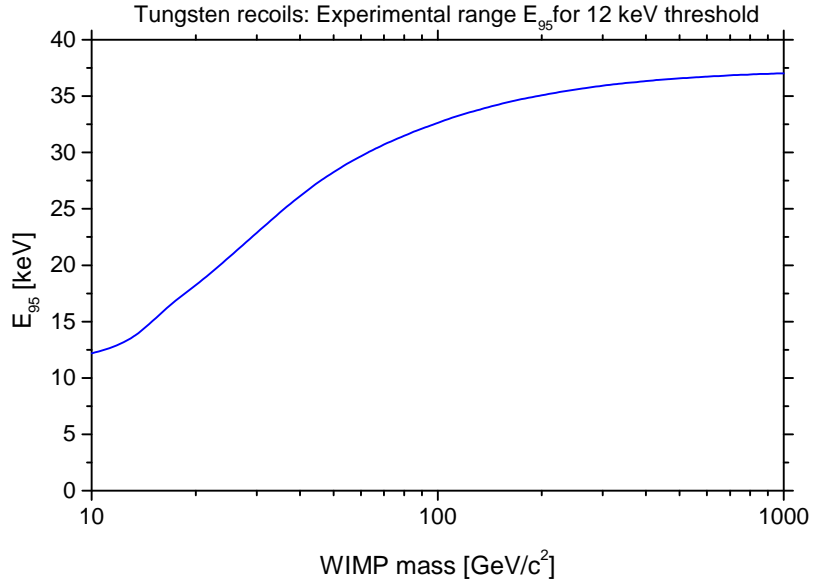


Figure 9: Recoil energy E_{95} for WIMP-tungsten elastic scattering as a function of WIMP mass. E_{95} is the recoil energy below which 95 % of the events above the threshold of 12 keV lie. The WIMP flux and nuclear form factor employed are described in the text.

If we nevertheless attribute all 16 events to WIMP interactions, we can set a conservative upper limit for the WIMP scattering cross section. We calculate such a limit for coherent (“spin independent”) interactions, assuming a standard halo model (isothermal halo, WIMP characteristic velocity: 220 km/s, mean Earth velocity: 232 km/s, local WIMP density: 0.3 GeV/c²/cm³). The Helm spin-independent form factor is used for the nucleus [16] with the parameterization suggested in Ref. [17] and A^2 scaling for coherence. The full line in Fig. 10 shows this limit calculated with the optimum interval method of ref. [18], together with the DAMA (1-4) 3 σ signal region [19] and exclusion limits from EDELWEISS [20] and CDMS [21]. Essentially identical results are obtained, when using each module separately.

3.2 Identification of the recoil nucleus

Further important improvements in our technique are to be anticipated if it were possible to use the information from the phonon-light output to identify which particular nucleus is recoiling. For neutrons in this recoil energy range our Monte Carlo simulation shows that the dominant scattering in the CaWO₄ is on the oxygen, with less than 5 % of the nuclear recoils due to tungsten. Hence the Q value derived from the neutron scattering experiment in ref. [7] is essentially determined by oxygen recoils. On the other hand for coherently interacting WIMPs the scattering is dominated by the tungsten, and a much higher value of Q may apply.

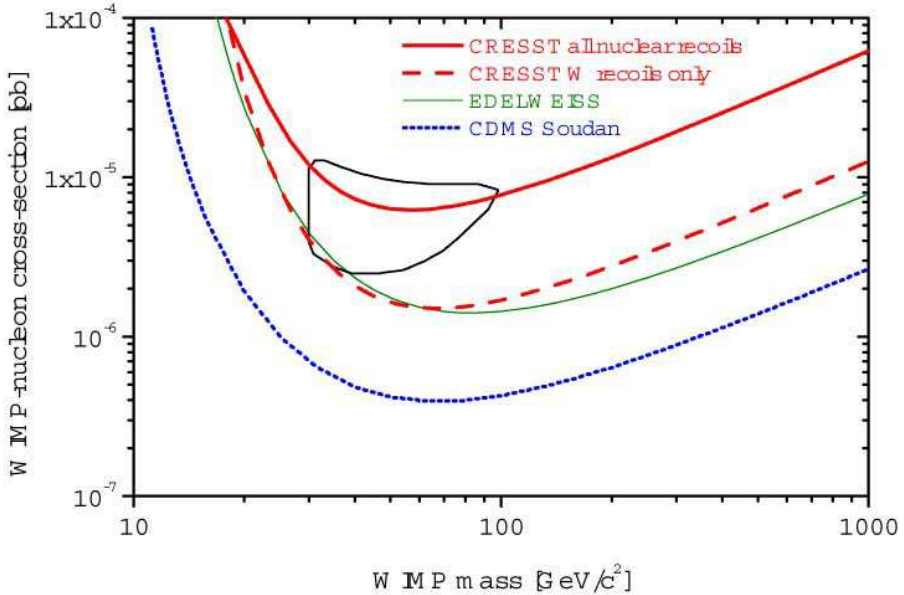


Figure 10: Coherent or spin independent scattering exclusion limits from the dark matter run. Using a quenching factor of $Q = 7.4$ to identify nuclear recoils as explained in the text we obtain the full curve. Using $Q = 40$ to identify tungsten recoils and the data of the better module Daisy/BE13 give the thick dashed line. Regions above the curves are excluded at 90 % CL. The enclosed region represents the claim of a positive signal by the DAMA collaboration [19].

For a better understanding of these matters, we have studied the quenching factors in CaWO_4 for the different recoil nuclei tungsten, calcium, and oxygen in a separate experiment. These measurements gave an extremely high quenching factor, between 40 and 50, for 18 keV and 36 keV tungsten energies. Such a high quenching factor will lead to no significant light for events with tungsten recoil energies below 40 keV. These quenching factor measurements were performed at room temperature and will be published in a separate paper [22]. Measurements at lower temperature, near 8 K, are in progress and seem to confirm these results. Despite the different experimental conditions we consider it worthwhile to analyze our data under the assumption that a quenching factor of $Q = 40$ applies for tungsten recoils. We then expect 90 % of the tungsten recoils to be below the full lines in Fig. 8.

One of the two modules (bottom in Fig. 8) has no recoil events below this full line in the energy range from 12 to 40 keV, while the other module has 3 events.

This difference between the two modules is presumably due to the better resolution in the light channel for the module with no events, which will inhibit “leakage” of neutron-induced recoils into the region of the tungsten events. This leakage can occur, for example,

when a statistical fluctuation in the light channel produces a low light value for a neutron-induced recoil. We can check the plausibility of this argument with an estimate of the “leakage”: Using the above determined resolutions with Gaussian fluctuations we calculate the probability, for each event in the neutron band, that it would have appeared below the tungsten line. This procedure leads to the following estimate for the leakage: for the module Daisy/BE13, 1.1 events; and for the module Julia/Be14, 3.6 events. Most of this leakage occurs at the lower energies where the tungsten acceptance line (solid line) lies above the 10 % boundary for the neutron recoils. If we were to move the analysis threshold from 12 to 25 keV the leakage would become much smaller, 0.092 and 0.62 events, respectively. Leakage does appear to give a plausible explanation for the behavior of the data in the tungsten recoil region.

If we now use the better module Daisy/BE13, where there are no tungsten events, to set a WIMP limit, we obtain the thick dashed line in Fig. 10. As a check we lowered the threshold to 10 keV to include the two events at 10.5 keV and 11.3 keV, below the tungsten line for Daisy/BE13 in Fig.8, and obtained essentially the same curve. This confirms the stability of the results against a variation of the analysis threshold,

At a WIMP mass of 60 GeV/c², these tungsten limits, which were obtained without any neutron shielding, are identical to the limits set by EDELWEISS [20] also assuming coherent interactions. Very recent results from CDMS at Soudan Underground Laboratory [21] have improved these limits by a further factor of four.

4 Summary and Perspectives

The present results were obtained without a neutron shield and the WIMP sensitivity appears to be limited by the neutron background when all nuclear recoil events in the CaWO₄ are naively attributed to WIMP interactions. However, we expect that the background neutrons, scattering predominantly on the light elements of the detector, lead to events distinguishable by light yield from coherently scattering WIMPs, which scatter predominantly on the tungsten. Thus if we exploit the very high quenching factor for tungsten, as recently measured at room temperature, the tungsten recoils can be separated. On this basis we have no tungsten recoils for the better of the two modules in the acceptance range of 12 to 40 keV. For the efficiency of this separation, the resolution of the light channel is crucial and the difference in the behavior of the two modules appears to be accounted for by the “leakage” of neutron-induced events in the module with the poorer resolution in the light channel.

We note that the coherent scattering hypothesis enters doubly in our analysis. Once, as for all types of detectors, in enhancing the rate on a heavy nucleus, given a certain WIMP-nucleon cross section. But secondly in a manner particular to the present method in that it leads to distinctly different anticipated light yields for neutron background and WIMP-induced recoils.

Finally we note that the method of identifying the recoil nucleus by the location of the

signal in the phonon-light plane seems very promising, not only for the suppression of background but also for the verification of a possible positive WIMP signal [6] and for unraveling the quantum numbers of a WIMP candidate [23]. To this end further study of quenching factors and improvement of the light detectors are being pursued.

5 Acknowledgements

This work was partially supported by the DFG SFB 375 “Teilchen-Astrophysik”, the EU Network “Cryogenic Detectors” (contract ERBFMRXCT980167), the EU Network HPRN-CT-2002-00322 “Applied Cryodetectors”, BMBF, PPARC, and two EU Marie Curie Fellowships.

References

- [1] M.W. Goodman and E. Witten, Phys. Rev. **D31** (1985) 3059.
- [2] A general review, including matters related to direct detection, may be found in G. Jungman, M. Kamionkowski, and K. Griest, Phys. Rep. **267** (1996) 195.
- [3] J. A. R. Caldwell and J. P. Ostriker, Ap. J. **251** (1981) 61. For a more recent discussion with a wider range of values see E. I. Gates, G. Gyuk, and M. S. Turner, Ap. J. **449** (1995) L123.
- [4] In general, coherent scattering will be characterized by the square of a linear combination of proton and neutron numbers. However we will follow the common practice and use $\sim A^2$.
- [5] G. Angloher et al., Astropart. Phys. **18** (2002) 43.
- [6] Update of the proposal to the LNGS for a second phase of the CRESST dark matter search, MPI-PhE/2001-02.
- [7] P. Meunier, M. Bravin, M. Bruckmayer, S. Giordano, M. Loidl, O. Meier, F. Pröbst, W. Seidel, M. Sisti, L. Stodolsky, S. Uchaikin and L. Zerle, Appl. Phys. Lett. **75** (1999) 1335.
- [8] P. DiStefano, T. Frank, G. Angloher, M. Bruckmayer, C. Cozzini, D. Hauff, F. Pröbst, S. Rutzinger, W. Seidel, L. Stodolsky and J. Schmidt, J. of Appl. Phys. **94** (2003) 6887.
- [9] G. Angloher et al., Proc. LTD-10, Nucl. Instrum. Meth. **A 520** (2004) 108-111.
F. Petricca, G. Angloher, C. Cozzini, T. Frank, D. Hauff, J. Ninkovic, F. Pröbst, W. Seidel, and S. Uchaikin, Proc. LTD-10, Nucl. Instrum. Meth. **A 520** (2004) 193.
- [10] M. F. Weber, C. Stover, L. Gilbert, T. Nevitt, and A. Onderkirk, Science **287** (2000) 2451.

- [11] F. Pröbst, M. Frank, S. Cooper, P. Colling, D. Dummer, P. Ferger, A. Nucciotti, W. Seidel, and L. Stodolsky, *J. Low Temp. Phys.* **100** (1995) 69.
- [12] M. Loidl, S. Cooper, O. Meier, F. Pröbst, G. Safran, W. Seidel, M. Sisti, L. Stodolsky, and S. Uchaikin, *Nucl. Instrum. Meth. A* **465** (2001) 440.
- [13] C. Cozzini et al., to be published.
- [14] N. Coron, G. Dambier, E. Leblanc, J. Leblanc, P. de Marcillac, and J.-P. Moalic, Proc. LTD-10, *Nucl. Instrum. Meth. A* **520** (2004) 159.
- [15] H. Wulandari, J. Jochum, W. Rau, F. von Feilitzsch, hep-ex/0401032, 21 Jan 2004, to be submitted to *Astropart. Phys.*
- [16] R. H. Helm, *Phys. Rev.* **104** (1956) 1466.
- [17] J. D. Lewin and P. F. Smith, *Astropart. Phys.* **6** (1996) 87.
- [18] S. Yellin, *Phys. Rev. D* **66** (2002) 32005.
- [19] R. Bernabei et al., *Phys. Lett. B* **480** (2000) 23.
- [20] A. Benoit et. al., *Phys. Lett. B* **545** (2002) 43.
- [21] D. S. Akerib et al., astro-ph/0405033, submitted to *Phys. Rev. Lett.*
- [22] J. Ninkovic et al., to be published.
- [23] See, for example, Fig. 24 of A. Gabutti, M. Olechowski, S. Cooper, S. Pokorski, and L. Stodolsky, *Astropart. Phys.* **6** (1996) 1.